JOURNAL OF GEOPHYSICAL RESEARCH, VOL. 111, D18104, doi:10.1029/2005JD006851, 2006

A general circulation model study of the orographic gravity waves over Antarctica excited by katabatic winds

Shingo Watanabe,[1] Kaoru Sato,[2] and Masaaki Takahashi[1,3]

Received 5 November 2005; revised 12 April 2006; accepted 13 June 2006; published 26 September 2006.

[1] In this study, we simulated orographic gravity waves (OGWs) over Antarctica using a T213L250 general circulation model (GCM). The GCM has a fine vertical resolution of 300 m throughout the middle atmosphere. The simulation was run for a 1-year period. Results from 21–28 June were primarily considered. OGWs are excited by katabatic winds that travel down the surface slopes of the Antarctic ice sheet. A strong eastward katabatic wind blows over the west coast of the Ross Sea at the approach of the synoptic-scale upper tropospheric westerly jets. A quasi-stationary OGW is then excited above the coast and propagates upward into the mesosphere. An OGW appears sporadically during the Antarctic winter and spring. Its amplitude is determined by the strength of the eastward katabatic wind. Dissipation of OGWs within the middle atmosphere results in a localized deceleration of westerly winds, greater than -30 m s^{-1} d^{-1}. This in turn modifies the horizontal circulation in the polar vortex. Strong vertical mixing occurs within the mesosphere and is associated with wave breaking. Large temperature fluctuations associated with the OGWs affect the formation or suppression of polar stratospheric clouds in the lower stratosphere. Katabatic wind excitation is the most powerful source of gravity waves over Antarctica around the time of the winter solstice.

Citation: Watanabe, S., K. Sato, and M. Takahashi (2006), A general circulation model study of the orographic gravity waves over Antarctica excited by katabatic winds, *J. Geophys. Res.*, *111*, D18104, doi:10.1029/2005JD006851.

1. Introduction

[2] Vertically propagating gravity waves are known to play an important role in the general circulation of the middle atmosphere [e.g., *Fritts and Alexander*, 2003]. These waves transport momentum and energy upward from the troposphere to the middle atmosphere where they are deposited. The deposition of momentum results in the acceleration of large-scale circulations. The waves have a wide variety of excitation mechanisms, including cumulus convection embedded in tropical storms and extratropical cyclones, as well as the dynamical instability of the tropospheric jet and the stratospheric polar night jet [e.g., *Sato*, 2000; *Fritts and Alexander*, 2003].

[3] Orographic gravity waves (OGWs) are quasi-stationary gravity waves excited by winds that move over land surfaces under stable stratification conditions. In the absence of time varying mean flows and strong flow nonlinearities, OGWs have a zero ground-based phase speed such that their dissipation always results in the deceleration of the background winds. At midlatitudes, OGWs are excited by the prevailing westerly surface winds as they travel over mountainous land surfaces. Some of the OGWs break above the extratropical tropopause and act to decelerate the westerly winds [e.g., *Sato*, 1994]. This deceleration plays an important role in separating the tropospheric subtropical jet from the stratospheric polar night jet [e.g., *Palmer et al.*, 1986; *McFarlane*, 1987; *Iwasaki et al.*, 1989]. The remaining OGWs break at a higher altitude and act to decelerate the wintertime mesospheric westerly jet.

[4] The surface circulation over Antarctica during winter is characterized by katabatic winds, that is, strong, cold flows of air running down the slopes of the Antarctic ice sheet [e.g., *Parish and Bromwich*, 1987]. The influence of the Coriolis Effect implies that the Antarctic katabatic winds generally have an anticyclonic or easterly wind component near the coast. OGWs are sometimes excited by katabatic winds because the ice sheet has an uneven topography, which includes steep cliffs along the coast. *Wu and Jiang* [2002] analyzed the radiance variances observed by the Upper Atmosphere Research Satellite Microwave Limb Sounder (UARS MLS) and found significant gravity wave activities along the Antarctic coastal region. OGWs appear to be an important source of such wave activities. In the present study, we used a high-resolution middle atmosphere general circu-

[1] Frontier Research Center for Global Change, Japan Agency for Marine-Earth Science and Technology, Yokohama, Japan.
[2] Department of Earth and Planetary Science, Graduate School of Science, University of Tokyo, Tokyo, Japan.
[3] Center for Climate System Research, University of Tokyo, Tokyo, Japan.

0148-0227/06/2005JD006851$09.00

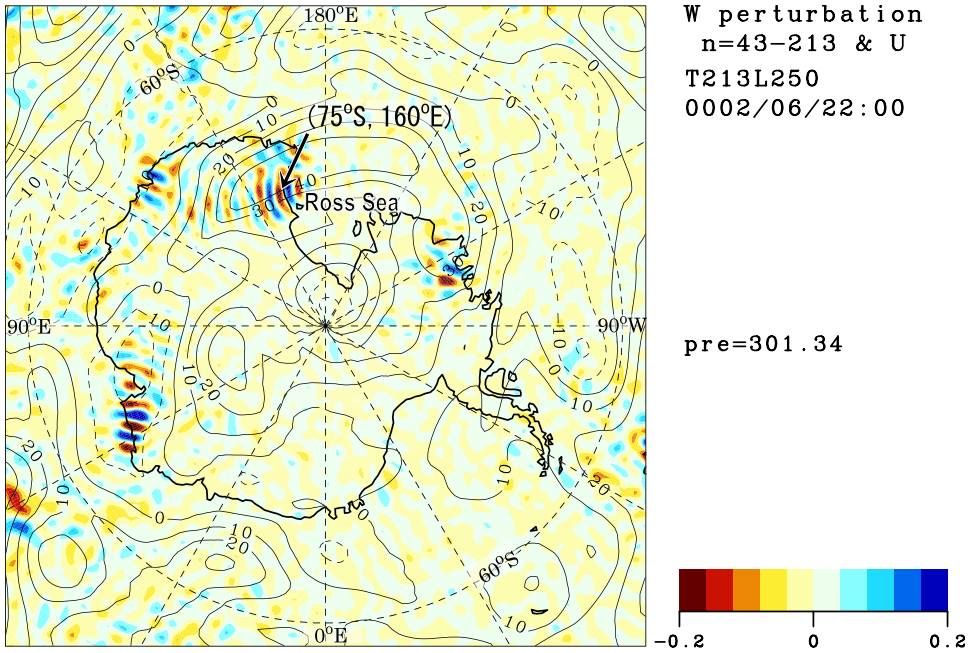

Figure 1. Horizontal distribution of those vertical velocity perturbations with a horizontal scale of less than 1000 km at 300 hPa [m s^{-1}]. Contour lines show background zonal wind at 300 hPa. The contour interval is 10 m s^{-1}.

lation model (GCM) to study OGWs over Antarctica and to explore their effects on the middle atmosphere.

2. Model and Experiment

[5] The GCM used in this study is an updated version of a model previously used for the study of gravity waves [e.g., *Kawatani et al.*, 2003, 2004; *Watanabe et al.*, 2005]. This GCM is a global spectral model that includes a realistic topography and a full set of physical processes [*K-1 Model Developers*, 2004]. An aquaplanet version of this GCM (T106L53) was used by *Sato et al.* [1999] to estimate the statistical characteristics of gravity waves as a function of latitude. The reality of gravity waves, in terms of wave structures and amplitudes, has been confirmed, since the observational data from a VHF clear air Doppler radar situated in Japan agrees with the model's results.

[6] In the present study, the top of the model is located slightly above 0.01 hPa (about 85 km). We used the climatological sea surface temperature and sea ice distribution. The terrain-following σ vertical coordinate system has been replaced by a hybrid σ pressure coordinate system following *Watanabe and Takahashi* [2005]. A terrain-following coordinate system gradually transforms into a pressure coordinate system in the troposphere. The pressure coordinate system starts at about 350 hPa. The horizontal resolution is T213, corresponding to a latitude-longitude grid interval of 0.5625°. The minimum horizontal wavelength resolved by this model is about 188 km. The GCM has 250 layers in the vertical direction, with a vertical resolution of 300 m throughout the middle atmosphere. The vertical layer thickness is reduced within the surface boundary layer, increases to about 750 m in the midtroposphere, and then returns to 300 m in the upper troposphere. The slightly coarser vertical resolution in the midtroposphere is necessary to obtain realistic convective precipitation using the Arakawa-Schubert cumulus parameterization. The high vertical resolution is important for realistically reproducing the equatorial quasi-biennial oscillation and semiannual oscillation, as well as wave propagation in background shear flows [*Watanabe and Takahashi*, 2005].

[7] Orographic and nonorographic gravity wave drag parameterizations are not included in the present simulation, since this study focuses on explicitly resolved gravity waves in the GCM. In the middle atmosphere, a Richardson-number-dependent vertical diffusion parameterization represents wave dissipation due to shearing instability. The dry convective adjustment represents wave dissipation due to convective instability. In order to obtain a realistic horizontal wave number spectrum of the small-scale motions, we used ∇^{16} hyperviscosity diffusion, which selectively suppresses energy at the smallest horizontal scales. The usual ∇^4 hyperviscosity diffusion, which has been used in previous studies, suppresses energy at the small and medium scales. In this study, the e-folding time for the smallest resolved motion is 0.8 day. A sponge layer is employed above 0.01 hPa, in which the wave motions are strongly damped. The sponge layer has 6 levels in which strength of the ∇^{16} horizontal diffusion is successively doubled to be 2, 4, 8, 16, 32, and 64 times as strong as the standard value. The total vertical thickness of the sponge layer is about 8 km. The time step is about 60 seconds. The initial conditions for the present simulation were based on the 1 October results of a T106L250 GCM simulation, which had been run for a 6-year period and was based on an isothermal atmosphere at rest. The T213L250 GCM was run for a 3-month period from 1 October to 1 January. The GCM was successively integrated over a period of one year, during which time the

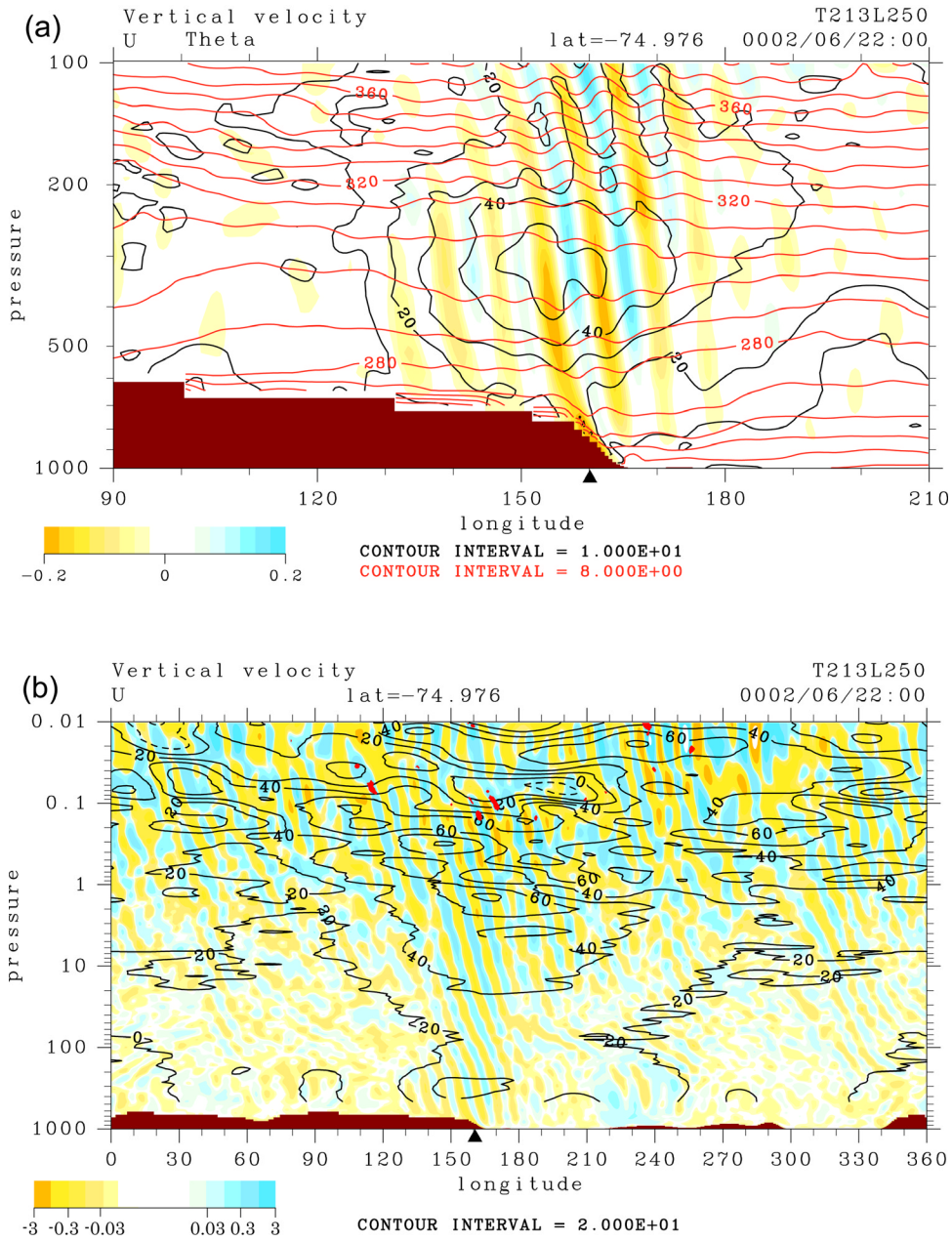

Figure 2. (a) Longitude-height cross section of the vertical wind [m s^{-1}] (color), background zonal wind [m s^{-1}] (black lines), and potential temperature [K] (red lines) at 75°S. (b) As for Figure 2a, but for the entire longitude and vertical domains. Color levels are set logarithmically. Red spots show regions of small (<0.25) Richardson number.

major meteorological elements were sampled every hour as hourly averages. Data in the terrain-following coordinate system were vertically interpolated to standard pressure levels before taking the averages.

[8] In this study, gravity waves are classified in terms of their horizontal scale. We focused on gravity waves with horizontal wavelengths of less than 1000 km. For this purpose, a spherical high-pass filter was applied to the original fields. The conversion procedure from the gridded fields to the spherical harmonics is identical to the Legendre transformation used in the GCM, which avoids any aliasing effects. Background fields are constructed as a sum of the zonal mean and the wave components larger than 1000 km. We concentrate our analysis on the Southern Hemisphere's winter solstice, when clearly defined OGWs appear over Antarctica. We also provide a brief discussion dealing with the seasonal variation in the occurrence of OGWs based on the full data set.

3. Results

3.1. Gravity Waves Over Antarctica

[9] Figure 1 shows the horizontal distribution of the filtered vertical wind perturbations at 300 hPa, on 22 June

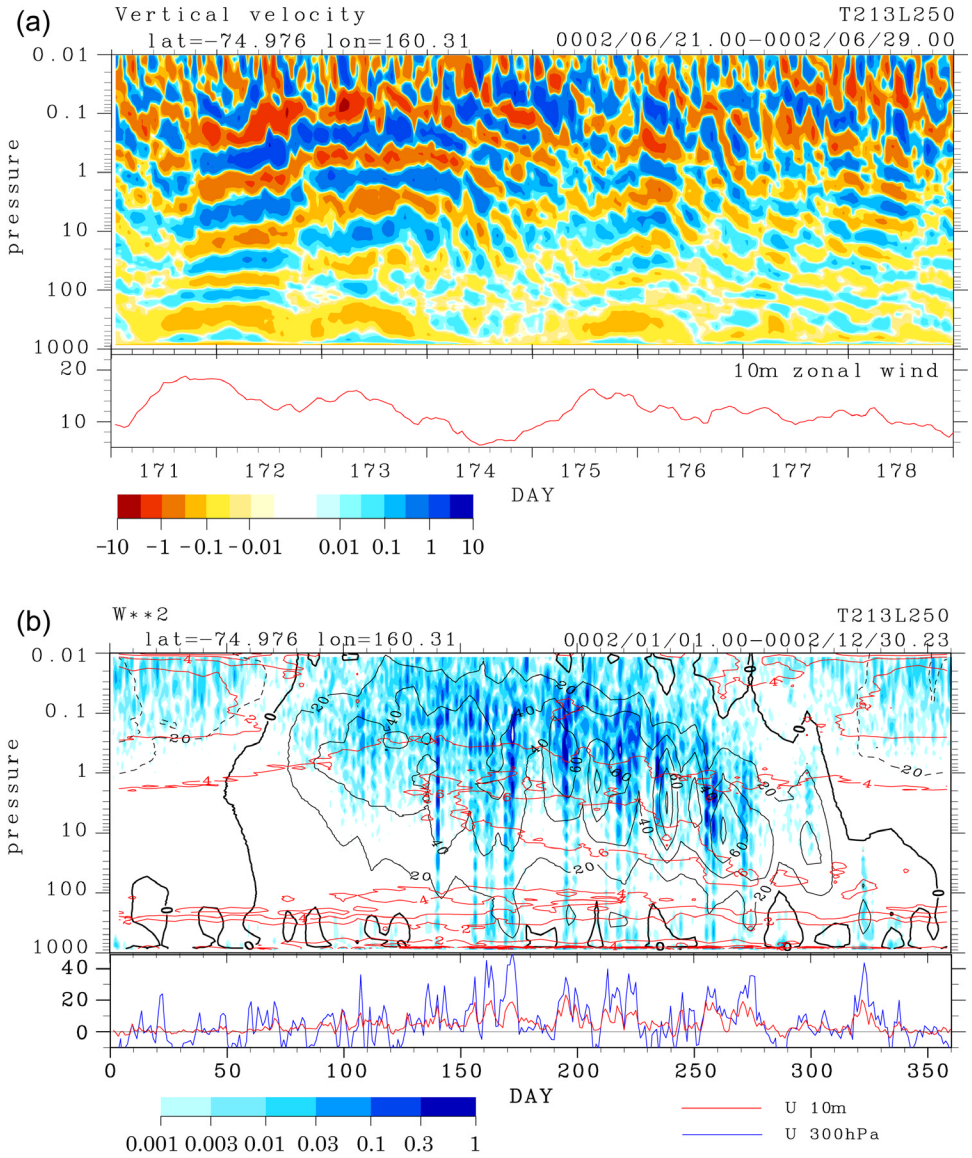

Figure 3. (a) (top) Time-height section of the vertical wind [m s^{-1}] at (75°S, 160°E). Color levels are set logarithmically. (bottom) Time series of eastward wind at 10 m above the surface [m s^{-1}]. (b) (top) Time-height section for variance of the vertical wind [m^2 s^{-2}]. Black shows background zonal wind [m s^{-1}]; red shows squared buoyancy frequency [$\times$ 10^{-4} s^{-2}]. (bottom) Time series of eastward wind at 10 m above the surface (red) and 300 hPa [m s^{-1}] (blue).

at 0000 UTC. Contour lines represent the background zonal wind at 300 hPa for the wind fields that have horizontal scales greater than 1000 km. A clear wave pattern is observed near the coast at 60°–90°E within a strong easterly wind where the wave propagation vector is oriented approximately parallel to the coast. The wave represents an OGW excited by an easterly katabatic wind on the ice sheet. Thus the wave is not observed at higher altitude in the stratospheric westerly winds (not shown). Another wave pattern is observed near the west coast of the Ross Sea, where the wave propagation vector is oriented approximately perpendicular to the coast. Since this gravity wave pattern is observed in a westerly tropospheric wind, it can propagate upward through the winter westerly winds into the stratosphere. We therefore focus our investigation on the generation mechanism of this particular OGW, as well as its effect upon the middle atmosphere.

3.2. Wave Generation and Structure

[10] Figure 2a shows the longitude-height distribution of the unfiltered vertical winds along 75°S in the vicinity of the west coast of the Ross Sea. Since the surface topography prevents the use of the spherical high-pass filter below about 450 hPa, we displayed the unfiltered vertical winds. The time of year is the same as that in Figure 1. Black contour lines represent the background westerly winds while the red contour lines represent the isentropes. A strong eastward, ($\sim$30 m s^{-1}) downslope ($\sim$0.25 m s^{-1}) flow or katabatic

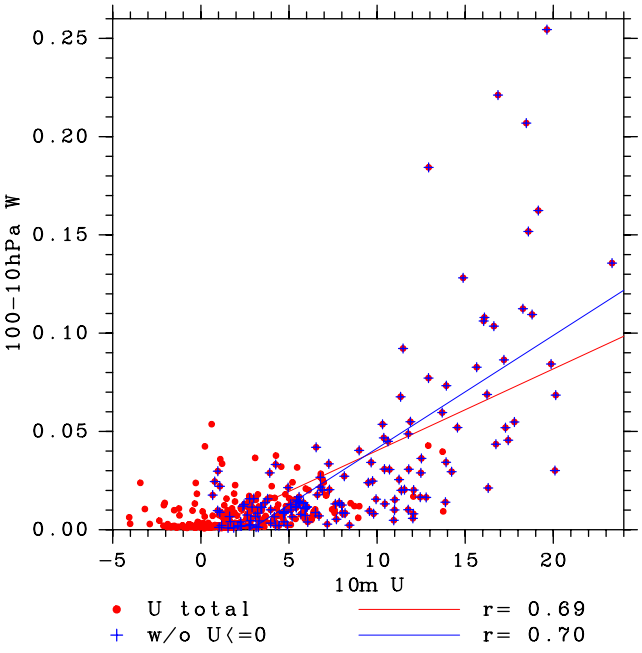

Figure 4. Scatter diagram of the katabatic wind speed [m s^{-1}] as a function of the amplitude of the vertical wind averaged over the 100–10 hPa [m s^{-1}] (see text). Blue crosses represent data on days when there are no critical levels below 100 hPa.

wind is observed along the coast, while a clear wave pattern extends downstream of the coast. The wave phases tilt westward with increasing altitude, which is characteristic of a westward propagating gravity wave relative to the background westerly wind. The distribution of the energy flux shows an upward propagation of gravity wave energy from the coast to the lower stratosphere (not shown), thus confirming that this wave is an OGW excited by a downslope katabatic wind.

[11] Figure 2b is similar to Figure 2a but covers the entire latitude circle and extends over the full vertical domain of the GCM. Red spots represent regions where the Richardson Number is less than 0.25, indicating the occurrence of a wave breaking in the model. The OGW propagates upward into the lower mesosphere and breaks down under an easterly wind region between 0.1 and 0.05 hPa. In the lower stratosphere, the horizontal wavelength is about 220 km, while the vertical wavelength is about 11 km. Some of the basic wave parameters are estimated using the dispersion relation of a gravity wave [e.g., *Fritts and Alexander*, 2003], considering the background condition for the buoyancy frequency and zonal wind. The estimated ground-based phase speed is approximately zero. In the lower stratosphere, the intrinsic period is about 2 hours, while the vertical group velocity is 3 km h^{-1}. The vertical group velocity increases in the upper stratosphere due to an increasing Doppler shift effect related to the background westerly winds. Hence the OGW reaches the lower mesosphere less than 10 hours after it is created in the troposphere (see Figure 3a, discussed in section 3.3). The amplitudes of the temperature fluctuations resulting from this OGW are approximately 5 K in the lower stratosphere and more than 10 K in the upper stratosphere and mesosphere (see below).

3.3. Dependence on the Katabatic Winds

[12] It is important to investigate the time evolution of the OGW and its dependence on the katabatic wind. Figure 3a shows the temporal evolution of vertical winds at the location (75°S, 160°E) over a period of 8 days, with eastward winds at

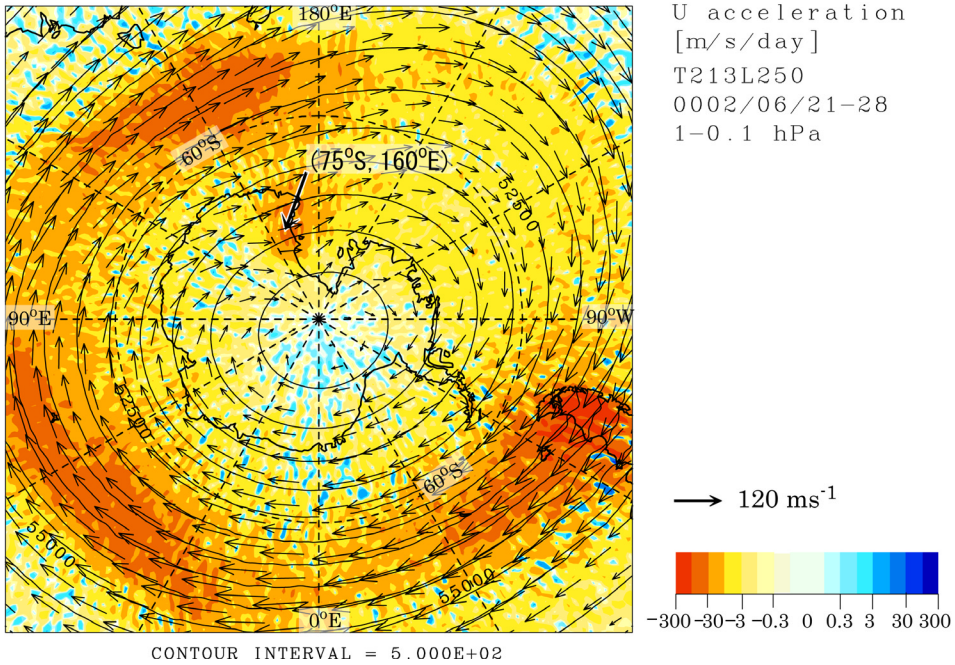

Figure 5. Zonal wind acceleration due to gravity waves, as averaged over 1–0.1 hPa [m s^{-1} d^{-1}]. Color levels are set logarithmically. Contours and arrows represent geopotential height and horizontal winds averaged over the same vertical interval.

10 m above the surface. The beginning of day 172 corresponds to the time in Figures 1 and 2. The excitation and vertical wavelength of the OGW are clearly controlled by the katabatic wind blowing down the slope (Figure 3a, bottom). As the zonal velocity of the katabatic wind exceeds $\sim$14 m s^{-1} at approximately 1000 UTC on day 171, the OGW is excited in the troposphere. The OGW propagates upward and reaches the mesosphere by about 2000 UTC. As the velocity of the katabatic wind decreases around 1000 UTC on day 172, the amplitude of the OGW also decreases. An OGW of similar amplitude and vertical wavelength again appears near the end of day 172 and lasts for about 24 hours. Another event occurs on day 175, when the surface westerly exceeds $\sim$14 m s^{-1}.

[13] We performed a similar analysis over the full year of the simulation to quantify the relationships between the energy of the OGW and the intensity of the katabatic wind. Figure 3b shows a time-height plot of the variance of the vertical velocity fluctuations ($\overline{w'^2}$), background zonal wind ($\bar{U}$), and buoyancy frequency squared (N^2). To clarify the key relationships, the daily average of $\overline{w'^2}$ and the 6-day averages of $\bar{U}$ and N^2 are shown. Time series data of 300 hPa eastward wind at the same location are added to Figure 3b (bottom), as the katabatic wind only develops when the synoptic-scale upper tropospheric westerly jet approaches the Ross Sea (see Figures 1 and 2a). It is clear that the OGWs appear throughout the winter and spring in the Antarctic, that is, from mid-May (day 140) to late November (day 323), whenever the westerly wind is dominant in the upper troposphere, and the eastward katabatic wind blows across the coast. On average, OGWs are excited about twice a month and last for about 1 to 4 days, although the wave structure varies with the strength of the katabatic wind, as can be seen in Figure 3a.

[14] Figure 4 shows a scatter diagram of the daily katabatic wind speed compared with the amplitude of the vertical velocity fluctuations averaged over 100–10 hPa. Figure 4 shows that there is a good correlation between the wind speed and amplitude, indicating that the signals apparent in Figure 3b are the OGWs. On days for which no critical level exists under 100 hPa (144 days, blue marks), the correlation coefficient is 0.70. The largest 13 events that had an average amplitude greater than 0.1 m s^{-1} occurred when the katabatic near surface wind speeds exceeded 13 m s^{-1}.

3.4. Effects of Gravity Waves on the Background Wind Fields

[15] Figure 5 shows the horizontal distribution of zonal wind accelerations resulting from gravity waves with horizontal wavelengths of less than 1000 km. Divergence of the vertical flux of zonal momentum is averaged over the vertical region of 1–0.1 hPa for 21–28 June. The polar vortex shows a zonal wave number 1 structure whose center shifts toward 30°W from the pole. The maximum westerly deceleration is observed near the mesospheric westerly jet (40°–50°S), and mainly results from the dissipation of nonorographic gravity waves excited over the ocean. However, over the tip of South America, OGWs are also important.

[16] A region of localized deceleration is also observed over the west coast of the Ross Sea, and is larger than -30 m s^{-1} d^{-1}. This deceleration results from the dissipation of the OGW. In this 8-day period, 21–28 June, small scale decelerations due to the dissipating OGW were continuously present above the west coast of the Ross Sea. Such a strong and localized deceleration acts as an obstacle to the horizontal flow and generates ageostrophic flows. Upstream of the deceleration, the wind vectors are deflected poleward of the geostrophic wind, while downstream of the deceleration, the wind vectors are deflected equatorward. (Similar flow deflection occurs upstream and near the tip of South America, where the mesospheric westerly jet is deflected poleward of the geostrophic wind.) These ageostrophic flows are important for horizontal transport in the polar vortex.

[17] There is a further possible role for the localized westerly deceleration. The zonal wave number 1 structure of the polar vortex results from a vertically propagating planetary wave probably forced in the midlatitude troposphere. In addition to the planetary wave, the deceleration over the west coast of the Ross Sea (centered around 160°E) helps to push the vortex center toward 20°W. It would be worthwhile to quantify the relative importance of the Antarctic OGW in forming the wave number 1 structure of the polar vortex. However, this is difficult to achieve solely on the basis of the results of the present study. A number of idealized numerical experiments are planned in which Antarctic and zonal asymmetries in the midlatitude surface conditions are removed from consideration.

3.5. Effects of OGWs on Tracer Transport and Chemistry

[18] In this section we investigate the effect on the transport and mixing of trace constituents in the lower mesosphere of OGWs that develop over the west coast of the Ross Sea. To achieve this, we performed a 10-hour forward trajectory calculation. The three-dimensional wind components are linearly interpolated to the tracer position. To minimize numerical diffusion of the trajectory, we used the fourth-order Runge-Kutta scheme with a time step of 60 seconds for the time integration [e.g., *Watanabe et al.*, 1999]. Figure 6a shows the 10-hour trajectory, beginning on 22 June at 0000 UTC. The tracers were initially placed at the 3000 K isentropic surface ($\approx$ 0.15 hPa). Horizontal transport due to the westerly wind of the polar vortex is dominant. The trajectories are not diffusive in a horizontal direction, even in the active wave region of the OGW (area on Figure 6a enclosed by the dashed circle). These results are consistent with those shown in Figure 5. Upstream of the wave region, the trajectories are directed mostly westward and slightly poleward, while the trajectories downstream of the wave region are directed equatorward.

[19] Figure 6b shows a longitude–potential temperature projection of the trajectories. Transport of the tracers is relatively conservative, in that they do not diverge significantly in a vertical direction outside the wave region (yellow and blue lines). In contrast, very large diffusive (cross isentropic) vertical mixing occurs in the wave region (red and black lines). Some of the strong vertical mixing is related to wave breaking events, which are easily identified in a longitude-height projection (Figure 6c). In the active wave region, very large (up to 4 km peak to peak) vertical displacements of the trajectories occur over very short time intervals.

[20] The OGW also affects the generation of polar stratospheric clouds (PSCs) in the winter polar vortex [e.g., *Carslaw et al.*, 1998; *Bacmeister et al.*, 1990; *Volkert and*

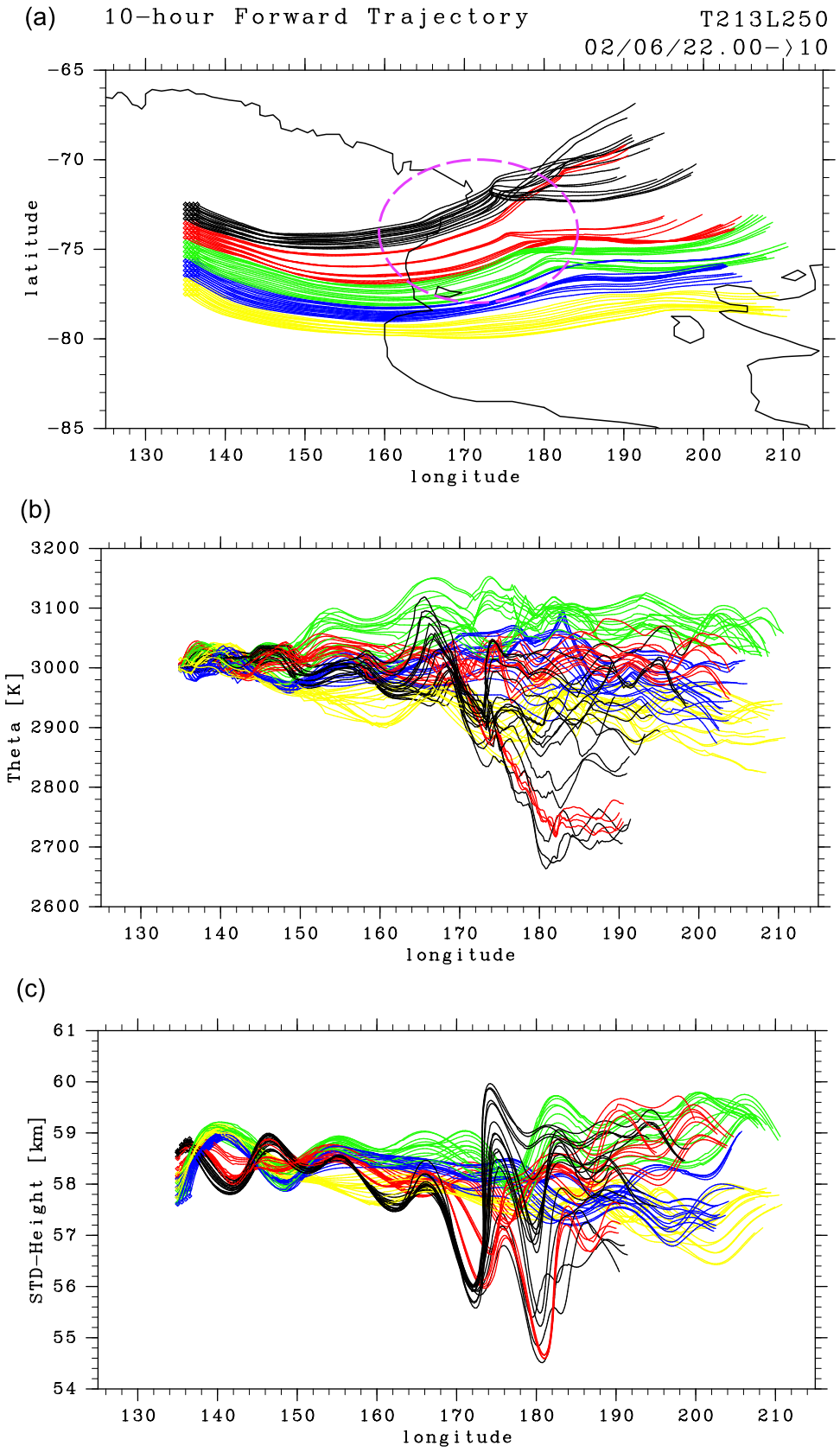

Figure 6. Ten hour forward trajectories of tracers calculated starting from 22 June at 0000 UTC. The trajectories are projected onto (a) a longitude-latitude plane, (b) a longitude–potential temperature plane, and (c) a longitude-height plane. Tracers were initially placed at the 3000 K isentrope (small circles).

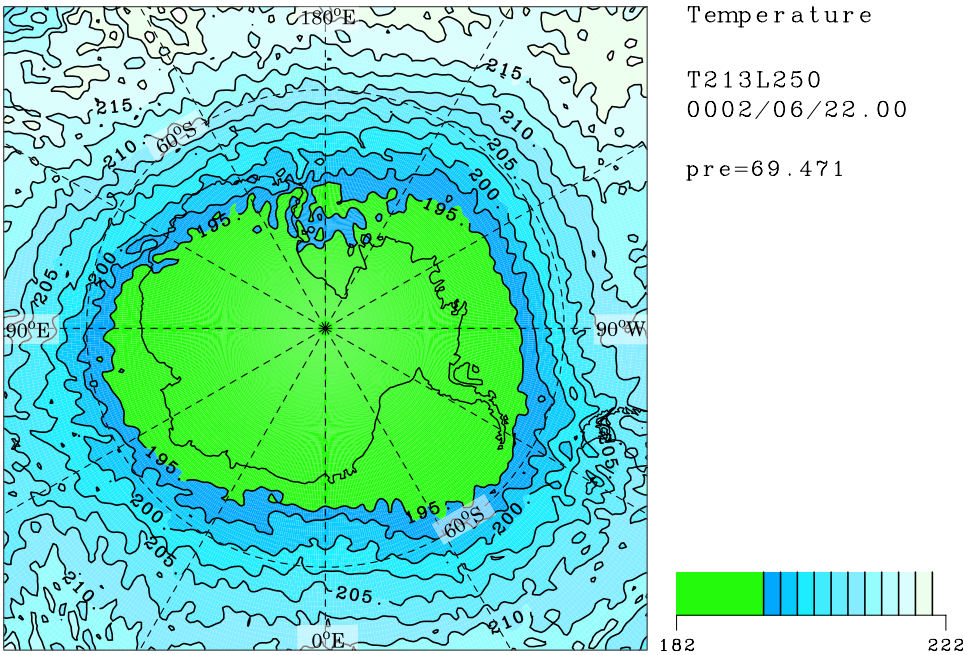

Figure 7. Temperature distribution at 70 hPa on 22 June at 0000 UTC. The contour interval is 2.5 K. Regions colder than the threshold temperature for ice-PSC formation, that is, with temperature less than 195 K, are highlighted in green.

Intes, 1992]. Figure 7 shows a polar map of the 70 hPa temperature on 22 June at 0000 UTC. Regions colder than the threshold temperature for ice-PSC formation, that is, areas colder than 195 K, are highlighted in green. Note that this GCM does not have a significant cold pole bias, which is a common problem in lower resolution GCMs. The large scale temperature distribution in the lower stratosphere is very similar to the observed distribution, such as detailed by the Met Office assimilation data [*Swinbank and A. O'Neill*, 1994]. At this time, the west coast of the Ross Sea corresponds to the inside edge of the cold polar vortex. It is possible that large positive temperature disturbances (∼+5 K) resulting from the OGW effectively suppress the formation of PSCs. In contrast, negative temperature disturbances associated with the OGW may assist PSC formation when the wave region is located outside the cold temperature vortex, that is, during the early winter and spring. The effects of the OGW on atmospheric chemistry in the Antarctic polar vortex have been studied for long time [e.g., *Cariolle et al.*, 1989; *Höpfner et al. 2005*]. It is worthwhile to quantify those effects using a high-resolution chemistry-coupled GCM that explicitly simulates OGWs. The effects of an Antarctic nonorographic gravity wave on the formation of PSCs are also worth investigating [e.g., *Shibata et al.*, 2003].

4. Discussion

[21] Our simulation, conducted using the T213L250 GCM, predicted the development of OGWs over Antarctica. The OGWs, and in particular the OGW that developed over the west coast of the Ross Sea, are excited by the katabatic wind that moves down the steep slope of the coastal area. *Wu* [2004] used radiance data collected by the AMSU-A instrument onboard NOAA satellites to estimate brightness temperature variances associated with mesoscale gravity waves, which typically have horizontal wavelengths of 50–200 km and vertical wavelengths of greater than 10 km. During June-August 2003 at ∼ 37 km, an isolated peak of a gravity wave was detected over the west coast of the Ross Sea (Figure 4, groups 2 and 5 of *Wu* [2004]). *Wu and Jiang* [2002] also showed a similar peak in the radiance variances that was observed by UARS MLS in August 1992. This peak was weaker in 1993 and totally absent in 1994. It is well known that the detectability of gravity wave signals by these instruments is significantly affected by background wind speeds, which change vertical wavelengths through Doppler shifting toward the limits of their detectable ranges [*Alexander*, 1998]. However, since the background flow is generally almost zonally symmetric in the Antarctic polar vortex, these observations likely indicate the dominance of gravity waves in the limited region over the west coast of the Ross Sea.

[22] The modeled excitation mechanism of the OGW and its effects on the middle atmosphere are likely to be at least qualitatively realistic. However, the characteristics of the modeled OGW are strongly dependent on the horizontal resolution of the GCM. To address this limitation, we considered the results of the finer-scale T1279L96 10 km mesh GCM simulation conducted by *Ofuchi et al.* [2004]. As the result of a trade-off between horizontal and vertical resolution, the vertical resolution of the T1279L96 GCM decreases with altitude, making it impossible to perform a thorough wave analysis from the land surface to the upper stratosphere. Hence we have mainly focused on the generation process and wave parameters in the troposphere.

[23] The T1279L96 GCM has similar OGWs to our study that are excited by the same mechanism as described in our GCM. However, they generally have smaller horizontal wavelengths that are approximately half the size of those in

our simulation (not shown). Regions of strong wave activity in the T1279 GCM are more confined to the coastal region than with our T213 result. This probably reflects the smaller horizontal wavelengths and finer topography of the finer-scale GCM. Further observations and high-resolution simulations are required to quantify the effects of the Antarctic OGW in the middle atmosphere in terms of the localized deceleration of the polar vortex, transport and mixing processes, and changes in chemical constituents resulting from temperature perturbations.

[24] *Yoshiki and Sato* [2000] analyzed operational radiosonde data from 21 stations at high-latitude sites in the southern hemisphere (15 stations in Antarctica), and determined the statistical characteristics of inertia gravity waves in the lower stratosphere. During the sudden stratospheric warming in 2002, CHAMP-GPS occultation measurements show the substantial potential energy of gravity waves in the lower stratosphere over Antarctica [*Ratnam et al.*, 2004a, 2004b]. These studies document springtime enhancements of gravity wave energy over the Antarctic lower stratosphere at the time that the center of the polar night jet descends from the upper stratosphere to the lower stratosphere and breaks down. Yoshiki and *Sato* [2000] suggested that the observed energy enhancement was partly due to modification by seasonal changes in background zonal wind and stability in the Antarctic lower stratosphere. In our simulation, the background static stability increases in the lower stratosphere during spring (see red contours in Figure 3b). As for the OGW that we considered in this study, the amplitude of vertical velocity fluctuations was controlled by the strength of the katabatic wind and was not significantly affected by background stability in the troposphere and lower stratosphere (Figures 3b and 4). We are currently undertaking a quantitative comparison of the gravity wave energy data obtained using our model results with observational measurements.

[25] It is also important to evaluate the relative importance of the Antarctic OGWs compared to those generated by other mechanisms, such as the dynamics of the polar night jet and synoptic-scale disturbances in the troposphere [*Sato*, 2000; *Yoshiki et al.*, 2004]. In terms of the winter solstice period discussed in the current study, the OGWs excited in the westerly katabatic wind over Antarctica have the largest amplitude found in any part of the troposphere and the middle atmosphere.

5. Summary

[26] Our high-resolution GCM simulation depicts the formation of a clear OGW over the west coast of the Ross Sea. The OGW is excited by the westerly katabatic wind that travels down the coastal slope and propagates up into the mesosphere. The OGW amplitude and vertical wavelength are controlled by the strength of the katabatic wind. The approach of the upper tropospheric westerly jet appears to be a necessary condition for the katabatic wind and wave generation. The OGWs sporadically occur throughout the Antarctic winter and spring, and last for about 1 to 4 days. In the middle atmosphere, the OGW modifies the horizontal wind in the polar region so that it departs from its geostrophic balance. This effect may play an important role in the horizontal transport in the polar vortex. The OGW also has a strong impact on vertical transport and mixing, especially in the mesosphere. When the OGW breaks, an air parcel is displaced by as much as 2 km depth, leading to strong cross-isentropic mixing. The OGW has large temperature fluctuations of approximately 5 K in the lower stratosphere. These can have a large effect on the formation and suppression of PSCs.

[27] **Acknowledgments.** The authors are grateful to W. Ofuchi and T. Enomoto at the Earth Simulator Center for kindly providing the results of the AGCM for the Earth Simulator (AFES) T1279L96 simulation. We also thank I. Hirota and three anonymous reviewers for their valuable comments. This work contributes to the project RR2002, MEXT, Japan. The calculations were conducted on the Earth Simulator. The GFD-DENNOU library and GTOOL were used for drawing the figures.

References

Alexander, M. J. (1998), Interpretations of observed climatological patterns in stratospheric gravity wave variance, *J. Geophys. Res.*, *103*, 8627–8640.

Bacmeister, J. T., M. R. Schoeberl, L. R. Lait, P. A. Newman, and B. Gary (1990), Small-scale waves encountered during AASE, *Geophys. Res. Lett.*, *17*, 4, doi:10.1029/90GL00050.

Cariolle, D., S. Muller, F. Cayla, and M. P. McCormick (1989), Mountain waves, polar stratospheric clouds, and the ozone depletion over Antarctica, *J. Geophys Res.*, *94*, 11,233–11,240.

Carslaw, K. S., M. Wirth, A. Tsias, B. P. Luo, A. Dornbrack, M. Leutbecher, H. Volkert, W. Renger, J. T. Bachmeister, and T. Peter (1998), Particle microphysics and chemistry in remotely observed mountain polar stratospheric clouds, *J. Geophys Res.*, *103*(D5), 5785–5796.

Fritts, D. C., and M. J. Alexander (2003), Gravity wave dynamics and effects in the middle atmosphere, *Rev. Geophys.*, *41*(1), 1003, doi:10.1029/2001RG000106.

Höpfner, M., et al. (2005), MIPAS detects Antarctic stratospheric belt of NAT PSCs caused by mountain waves, *Atmos. Chem. Phys.*, *6*, 1221–1230.

Iwasaki, T., S. Yamada, and K. Tada (1989), A parameterization scheme of orographic gravity wave drag with two different vertical partitionings. Part I: Impacts on medium-range forecasts, *J. Meteorol. Soc. Jpn.*, *67*, 11–27.

K-1 Model Developers,(2004), K-1 coupled model (MIROC) description, technical report, vol. 1, edited by H. Hasumi, and S. Emori. 34 pp., Cent. for Clim. Sys. Res., Univ. of Tokyo.

Kawatani, Y., S. K. Dhaka, M. Takahashi, and T. Tsuda (2003), Large potential energy of gravity waves over a smooth surface with little convection: Simulation and observation, *Geophys. Res. Lett.*, *30*(8), 1438, doi:10.1029/2003GL016960.

Kawatani, Y., M. Takahashi, and T. Tokioka (2004), Gravity waves around the subtropical jet of the southern winter in an atmospheric general circulation model, *Geophys. Res. Lett.*, *31*, L22109, doi:10.1029/2004GL020794.

McFarlane, N. M. (1987), The effect of orographically excited gravity wave drag on the general circulation of the lower stratosphere and troposphere, *J. Atmos. Sci.*, *44*(14), 1775–1800.

Ofuchi, W., H. Nakamura, M. K. Yoshioka, T. Enomoto, K. Takaya, X. Peng, S. Yamane, T. Nishimura, Y. Kurihara, and K. Ninomiya (2004), 10-km mesh meso-scale resolving simulations of the global atmosphere on the Earth Simulator – Preliminary outcomes of AFES (AGCM for the Earth Simulator), *J. Earth Simulator*, *1*, 8–34.

Palmer, T. N., G. J. Shutts, and R. Swinbank (1986), Alleviation of a systematic westerly bias in general circulation and numerical weather prediction models through an orographic gravity wave drag parameterization, *Q.J.R. Meteorol. Soc*, *112*, 1001–1039.

Parish, T. R., and D. H. Bromwich (1987), The surface windfield over the Antarctic ice sheets, *Nature*, *328*, 51–54.

Ratnam, M. V., G. Tezlaff, and C. Jacobi (2004a), Global and seasonal variations of stratospheric GW activity deduced from the CHAllenging Minisatellite Payload (CHAMP)-GPS Satellite, *J. Atmos. Sci.*, *61*, 1610–1620.

Ratnam, M. V., T. Tsuda, C. Jacobi, and Y. Aoyama (2004b), Enhancement of gravity wave activity observed during a major Southern Hemisphere stratospheric warming by CHAMP/GPS measurements, *Geophys. Res. Lett.*, *31*, L16101, doi:10.1029/2004GL019789.

Sato, K. (1994), A statistical study of the structure, saturation and sources of inertio-gravity waves in the lower stratosphere observed with the MU radar, *J. Atmos. Terr. Phys.*, *56*, 755–774.

Sato, K. (2000), Sources of gravity waves in the polar middle atmosphere, *Adv. Polar Upper Atmos. Res.*, *14*, 233–240.

Sato, K., T. Kumakura, and M. Takahashi (1999), Gravity waves appearing in a high-resolution GCM simulation, *J. Atmos. Sci.*, *56*, 1005–1018.

Shibata, T., K. Sato, H. Kobayashi, M. Yabuki, and M. Shiobara (2003), Antarctic polar stratospheric clouds under temperature perturbation by nonorographic intertia gravity waves observed by micropulse lidar at Syowa Station, *J. Geophys. Res.*, *108*, 4105, doi:10.1029/2002JD002713.

Swinbank, R., and A. O'Neil (1994), A stratosphere-troposphere data assimilation system, *Mon. Weather Rev.*, *122*, 682–702.

Volkert, H., and D. Intes (1992), Orographically forced stratospheric-waves over northern Scandinavia, *Geophys. Res. Lett.*, *19*, 1205–1208.

Watanabe, S., and M. Takahashi (2005), Kelvin waves and ozone Kelvin waves in the QBO and SAO; a simulation by a high-resolution chemistry-coupled GCM, *J. Geophys. Res.*, *110*, D18303, doi:10.1029/2004JD005424.

Watanabe, S., S. Miyahara, and Y. Miyoshi (1999), Lagrangian transport experiments in the MLT region, *Earth Planets Space*, *51*, 745–750.

Watanabe, S., T. Nagashima, and S. Emori (2005), Impact of global warming on gravity wave momentum flux in the lower stratosphere, *SOLA*, *1*, 189–192, doi:10.2151/sola.2005-049.

Wu, D. L. (2004), Mesoscale gravity wave variances from AMSU-A radiances, *Geophys. Res. Lett.*, *31*, L12114, doi:10.1029/2004GL019562.

Wu, D.L., and J.H. Jiang (2002), MLS observations of atmospheric gravity waves over Antarctica, *J. Geophys. Res.*, *107*(24), 4773, doi:10.1029/2002JD002390.

Yoshiki, M., and K. Sato (2000), A statistical study of gravity waves in the polar regions based on operational radiosonde data, *J. Geophys. Res.*, *105*(D14), 17,995–18,011.

Yoshiki, M., N. Kizu, and K. Sato (2004), Energy enhancements of gravity waves in the Antarctic lower stratosphere associated with variations in the polar vortex and tropospheric disturbances, *J. Geophys. Res.*, *109*, D23104, doi:10.1029/2004JD004870.

K. Sato, Department of Earth and Planetary Science, Graduate School of Science, University of Tokyo, Tokyo 113-0033, Japan.

M. Takahashi and S. Watanabe, Frontier Research Center for Global Change, Japan Agency for Marine-Earth Science and Technology, 3173-25 Showa-machi, Kanazawa-ku, Yokohama-city, Kanagawa 236-0001, Japan. (wnabe@jamstec.go.jp)